Supplemental Material
Identification of prompt-proton emission in $N = Z$–1 ^{61}Ga: isospin symmetry at the limit of nucler binding

The Supplemental Material provides details on the experimental set-up, data acquisition, and data analysis of the identified proton-emission line associated with the decay of the proton $\pi g_{9/2}$ single-particle state in ^{61}Ga. It further describes complementing the JUN45 $f_{5/2}pg_{9/2}$ interaction [46] with isospin-breaking terms for use with the ANTOINE shell-model code [41,42]. (The numbering of references in this Supplemental Material corresponds to references in the main article.)

I. DETAILS OF THE EXPERIMENTAL SET-UP

Figure 1 shows a sketch of the experimental set-up, where the special detector arrangement inside the target chamber is highlighted. It contains eight out of the nine rings of Microball CsI(Tl) detector elements (R1-R3, R5-R9). Ring R4, usually comprising 12 CsI(Tl) detector elements, was removed to give space for two CD-shaped double-sided silicon strip detectors (DSSD 1 and DSSD 2) mounted at forward angles with respect to the beam direction. The arrangement thus left 83 out of 95 CsI(Tl) detectors, of which 75 were operational during the experimental campaign. According to Fig. 1, Microball rings R1 and R5-R9 operated regularly, while ring R3 provided E detection capability behind DSSD 1 in case high-energy evaporated protons or deuterons penetrated the latter. Similarly, R2 elements could detect remaining energies for particles penetrating both DSSD 1 and DSSD 2.

DSSD 1 was placed 32 mm downstream of the target position, covering laboratory angles between $\theta_1 = 12°$ and $\theta_2 = 53°$ relative to the beam direction. DSSD 2 was placed 40 mm downstream of DSSD 1. The DSSDs were protected against scattered heavy-ion beam particles by (*i*) a set of tantalum absorber rings, decreasing in thickness as a function of angle, θ, with respect to the beam direction (see Table I), and (*ii*) a tantalum cone placed between the physical inner holes of the two DSSDs. These rings had an opening of 7 mm in diameter, allowing recoils to enter the Fragment Mass Analyzer (FMA) in a cone of $\theta \approx \pm 6.5°$ ($\Omega \approx 40$ msr). The FMA was set to accept recoils of mass $A = 60, 61, 62$ with $q = 16^+$ and kinetic energies $E = 54$ MeV.

Figure 2 shows a drawing of the silicon wafer of DSSD 1. For details, see the figure caption. Its 310 μm thick wafer is embedded into a printed circuit board (PCB) which has an outer diameter of 130.0 mm. The PCB holds six 34-pin connectors for the processing of the $64 + 32 = 96$ electronics channels of each DSSD. DSSD 2 is 520 μm thick with a physical inner diameter of 28 mm, an active inner diameter of 32 mm, and an equal width of all 32 rings of $((85\,\text{mm} - 32\,\text{mm})/2)/32 = 0.83$ mm.

TABLE I: Details on the stack of tantalum absorber foils placed in front of DSSD 1. Diameter indicates inner diameter of an individual foil labeled with a number. Individual and accumulated thicknesses of the foils are presented.

Absorber number	1	2	3	4	5
Diameter (mm)	7	10	28	40	60
Individual thickness (μm)	30.0	7.5	5.0	7.5	12.5
Accumulated thickness (μm)	62.5	32.5	25.0	20.0	12.5

With a pixelation of $32 \times 64 = 2048$ each, DSSD 1 and DSSD 2 form a novel, highly-pixelated ΔE-E charged-particle identification and tracking system for high-resolution in-beam particle-γ coincidence spectroscopy. This system was combined with Gammasphere, which comprised 71 Ge-BGO modules. The 32 most forward modules were replaced by liquid scintillator detectors of the Neutron Shell. The FMA collected information on the mass-to-charge ratio, A/q, of recoiling nuclei with a position-sensitive parallel grid avalanche counter (PPAC) at the focal plane, and on their atomic number, Z, with the help of an ionization chamber (IC).

II. MORE ON THE ^{61}GA PROTON LINE

Figure 3 complements Fig. 2 of the main article showing the γ-ray spectrum in coincidence with $E_p = [1.75, 2.05]$ MeV (dark blue) in the energy range covering tentative transitions in addition to the main 958-keV line. The normalized background spectrum (gray) is obtained by selecting coincidences with protons satisfying $E_p = [1.50, 1.75]$ or $E_p = [2.05, 3.50]$ MeV. Two tentative γ-ray transitions are suggested at 1039(2) and 1697(2) keV. Even though 1039-keV and 1697-keV selected proton spectra have a low number of counts, they could be summed with the 958-keV spectrum [cf. Fig. 4(c)]. That spectrum is shown in Fig. 4(d). Its proton peak at 1.9 MeV has twice the yield compared with Fig. 4(c), supporting the additional tentative coincidences.

Figure 4 complements Fig. 3 of the main article, which is included as panel (c). All panels in Fig. 4 involve the requirement of a mass $A = 60$ recoil detected in the FMA as well as a γ-ray multiplicity $k > 3$. Panels (a)-(f) require $N_p = 1, 2$ detected protons, panels (g) and (h) $N_p \geq 3$. At least one of the detected protons had to be detected solely by DSSD 1. Panels (a) and (b) in Fig. 4 are *without* the tracking correction of the beam-spot position throughout the experiment. There is a clear improvement in peak shape comparing panels (c)

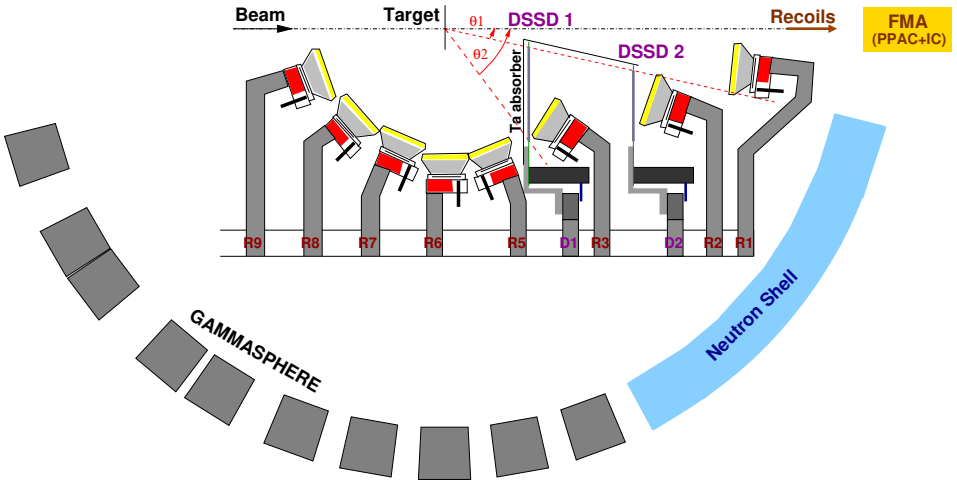

FIG. 1: Sketch of the experimental set-up, highlighting the arrangement of the combination of eight rings of Microball CsI(Tl) detector elements with two CD-shaped double-sided silicon strip detectors (DSSD 1 and DSSD 2) inside the target chamber. The chamber is surrounded by Gammasphere modules (gray) and liquid scintillator Neutron Shell elements (blue). Recoils are allowed to enter the Fragment Mass Analyzer (FMA) to collect information on their mass-to-charge ratio, A/q, with a position-sensitive parallel grid avalanche counter (PPAC) as well as their atomic number, Z, with the help of an ionization chamber (IC). See text for more details.

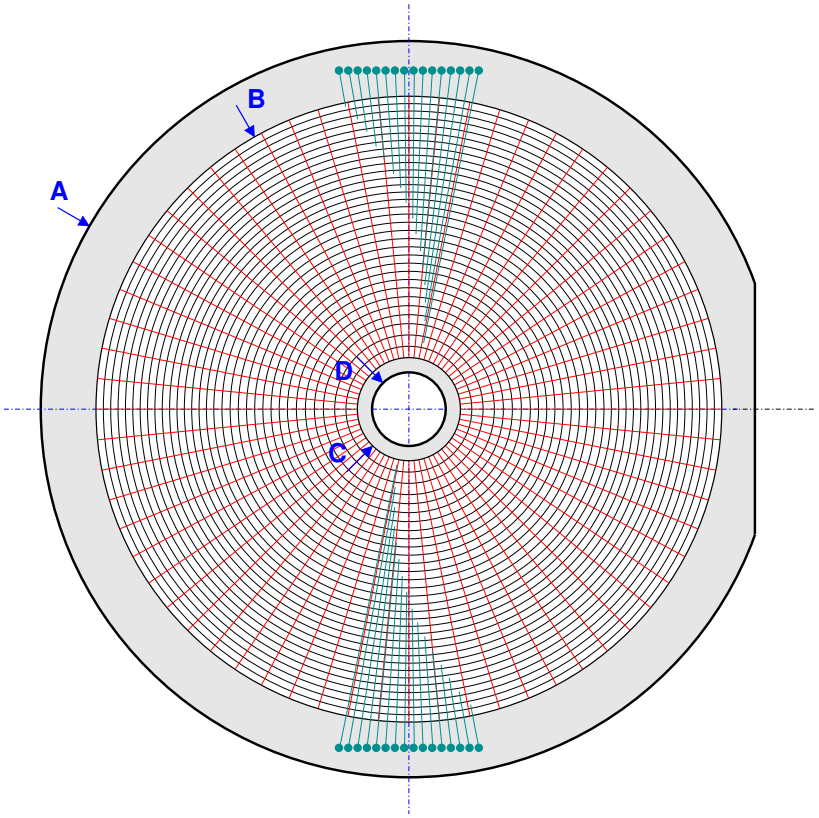

FIG. 2: Technical details of the silicon wafer of CD-DSSD1. Its physical outer and inner diameters are $A = 100.0$ mm and $D = 10.0$ mm, respectively. The active area has an outer diameter of $B = 85.0$ mm and an inner diameter of $C = 14$ mm. The n-side (ohmic) is segmented into 32 rings having widths of 1.6 (3×), 1.2 (4×), 1.1 (9×), and 1.0 mm (16×), counting from the inner to outer part of the DSSD. The p-side (junction) is divided into 64 segments indicated by the red lines. Bonding pads for the 32 rings are indicated by the dots in cyan, alternatingly connected to rings with 16 pads each on top and at the bottom.

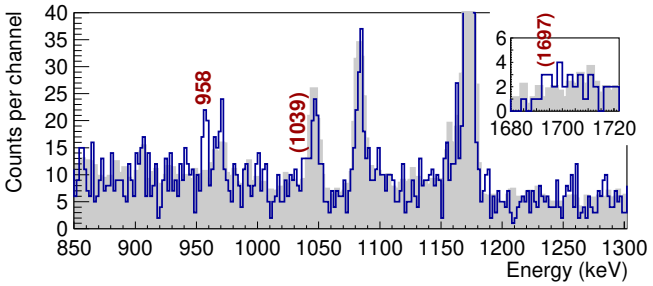

FIG. 3: Measured γ-ray energy spectrum (blue) plotted in coincidence with $E_p = [1.75, 2.05]$ MeV. The background is depicted in gray. The spectrum is the same as Fig. 2 of the main article, but covers a larger energy range. Two tentative transitions at 1039(2) and 1697(2) keV are suggested in addition to the firm 958-keV peak. Transitions of interest are labeled with their energy in keV. The binning is 1 keV per channel.

with (a) and (d) with (b), respectively, i.e., by including beam-spot tracking in the transformation of proton energies from the laboratory into the center-of-mass frame. Background-subtracted spectra are shown in Fig. 4(e) and (f). These panels also include the results of a Gaussian least-squares peak fit. The obvious disappearance of the proton line in panels (g) and (h) assures the assignment of the proton line to arise from a decay of an excited state in ^{61}Ga, because ^{61}Ga is produced in the $1p2n$ reaction channel, i.e., a maximum of two protons, $N_p = 2$, can be detected in this case, namely one evaporated proton and one proton connecting the excited state in ^{61}Ga with the ground state of ^{60}Zn.

III. GEANT4 SELF-CONSISTENCY CHECK

Figure 5 provides the results of Geant4 simulations which were conducted to ensure "self-consistency" in correcting data for energy losses in the Ta absorber foils as well as transforming proton energies from the laboratory into the center-of-mass frame for emission from moving ^{61}Ga nuclei. For this purpose, ^{61}Ga was produced at different depths in the 0.43 mg/cm^2 thick ^{24}Mg target foil and protons with a fixed $Q_{p,\mathrm{in}} = 2.000$ MeV were sent into the detection system illustrated in Fig. 1. Following energy loss in the Ta absorbers, proton energy distributions seen by DSSD 1 are shown in Fig. 5(a) and resolved for detection angle in panel (b). In the following, events in these spectra were treated identically to the routine applied to the observed candidate events. First, the spectra are corrected for the varying Ta absorber thicknesses. The results are provided in Fig. 5(c) and as a function of detection angle, θ, in Fig. 5(d). Finally, the transformation from laboratory to center-of-mass frame is conducted, which leads to the spectra in Fig. 5(e) and (f). Panel (f) shows that the deduced proton energies are independent of laboratory angle, θ. Further, a Gaussian least-squares peak fit provides $E_p = 1.968(1)$ MeV, which is perfectly consistent with $Q_{p,\mathrm{in}} = 2.000$ MeV. These simulations justify the data analysis procedures and thus ensure that derived proton energies (cf. Fig. 4) are essentially free from systematic uncertainties.

IV. ISOSPIN-BREAKING JUN45 INTERACTION

The present study of isospin-breaking effects requires the introduction of isospin-breaking terms into the underlying shell-model interaction. This concerns Coulomb energies to be added to proton-proton two-body matrix elements (TBME) as well as modifications of proton and neutron single-particle energies (SPE). It has been done for the JUN45 interaction [46]. The modifications are summarized in Tables II and III.

The Coulomb multipole contributions, V_{CM} ("coul"), have been calculated for harmonic-oscillator wave functions using $\frac{m\omega}{\hbar} = (45A^{-1/3} - 25A^{-2/3})/42.75 = 0.2329 fm^{-2}$ for $A = 58$ in the modified JUN45 interaction. The corresponding parametrization reproduces established V_{CM} in the fp shell ($A = 42$).

Concerning SPE, first well-defined $V_{C\ell s}$ ("SO") contributions [2] were added as well as $V_{Cr}(p_{3/2}) - V_{Cr}(f_{7/2}) = -300$ keV, based on experimental mass $T_z = \pm 1/2$, $A = 41$ single-particle energies ("VR"). Then

- $V_{Cr}(f_{5/2}) - V_{Cr}(p_{3/2}) = +80$ keV,
- $V_{Cr}(p_{1/2}) - V_{Cr}(p_{3/2}) = -110$ keV, and
- $V_{Cr}(g_{9/2}) - V_{Cr}(p_{3/2}) = -80$ keV,

i.e., with respect to the $f_{7/2}$ SPE

- $V_{Cr}(f_{5/2}) = -220$ keV,
- $V_{Cr}(p_{1/2}) = -410$ keV, and
- $V_{Cr}(g_{9/2}) = -380$ keV,

were implemented to describe the known MED of the anticipated $1/2^-$, $5/2^-$, and $9/2^+$ single-particle states in the $T_z = \pm 1/2$, $A = 57$ mirror pair ^{57}Cu and ^{57}Ni. For the $f_{5/2}$ and $p_{1/2}$ orbitals, these numbers are in the range of values discussed in, e.g., Ref. [2]. Finally, the centroids of proton and neutron SPE were normalized ("n") to maintain the original JUN45 values for $p_{3/2}$, $f_{5/2}$, $p_{1/2}$, and $g_{9/2}$ orbitals, respectively.

Based on JUN45coul_SOVRn predictions for the $T = 1$ 0^+, 2^+, and 4^+ states in the $A = 58$ triplet (^{58}Zn, ^{58}Cu, and ^{58}Ni), no specific isovector isospin-nonconserving matrix elements needed to be included in the interaction file, different from interactions in the fp space (see, e.g., Ref. [50]). For $A = 58$, $\mathrm{TED}_{\mathrm{exp}}(2^+) = -88$ keV and $\mathrm{TED}_{\mathrm{exp}}(4^+) = -136$ keV. For JUN45coul_SOVR, $\mathrm{TED}(2^+) = -85$ keV and $\mathrm{TED}(4^+) = -122$ keV, and only the latter changing slightly to $\mathrm{TED}(4^+) = -120$ keV for JUN45coul_SOVRn. Potential corrections for isospin triplet effects are not crucial for the present study.

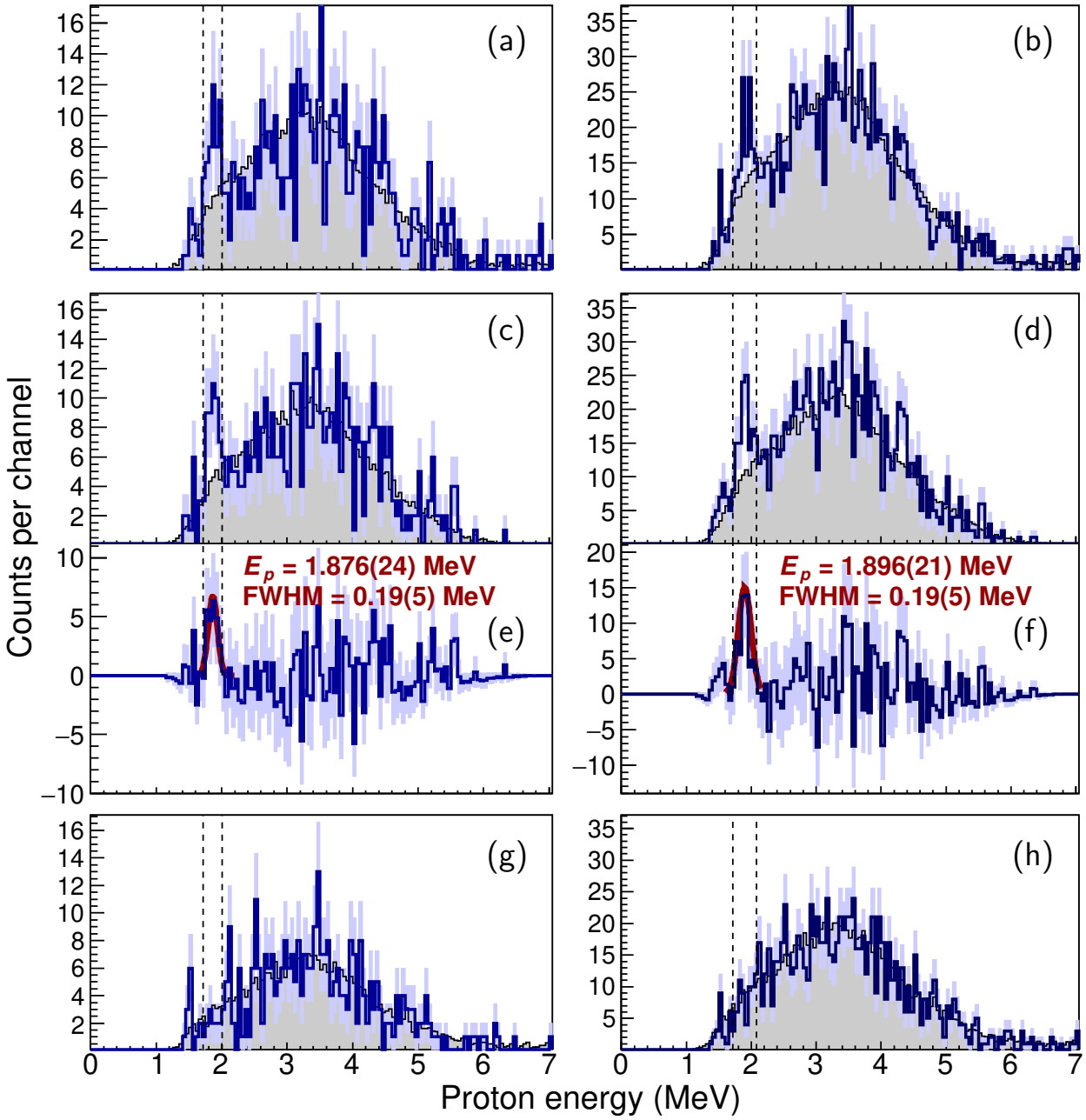

FIG. 4: Proton energy spectra (dark blue) in coincidence with the 958-keV γ-ray transition (left panels) and with the sum of the 1697-, 1039-, and 958-keV γ-ray transitions (right panels) associated with ^{61}Ga. All spectra are pre-selected by mass $A = 60$ and γ-ray multiplicity $k = 3$. The top panels (a) and (b) show proton energies computed in the center-of-mass frame assuming a perfectly centered beam. Panel (c) is the same spectrum as the one in Fig. 2 of the main article. Panels (c) and (d) show the proton energies with beam offsets taken into account for proton-energy corrections. Panels (e) and (f) show proton energy spectra after background subtraction together with the results of a Gaussian least-squares fit. The required total number of protons per event for the top three rows is $1 \leq N_p \leq 2$. The bottom row shows the result of changing this and only this requirement to $N_p \geq 3$. Spectra in black correspond to normalized background arising from coincidences with $E_\gamma = [900, 1100]$ keV. Areas in light blue indicate statistical uncertainties per channel. The binning is 50 keV per channel. Dashed vertical lines guide the eye along the proton peak position at $E_p \approx 1.9$ MeV.

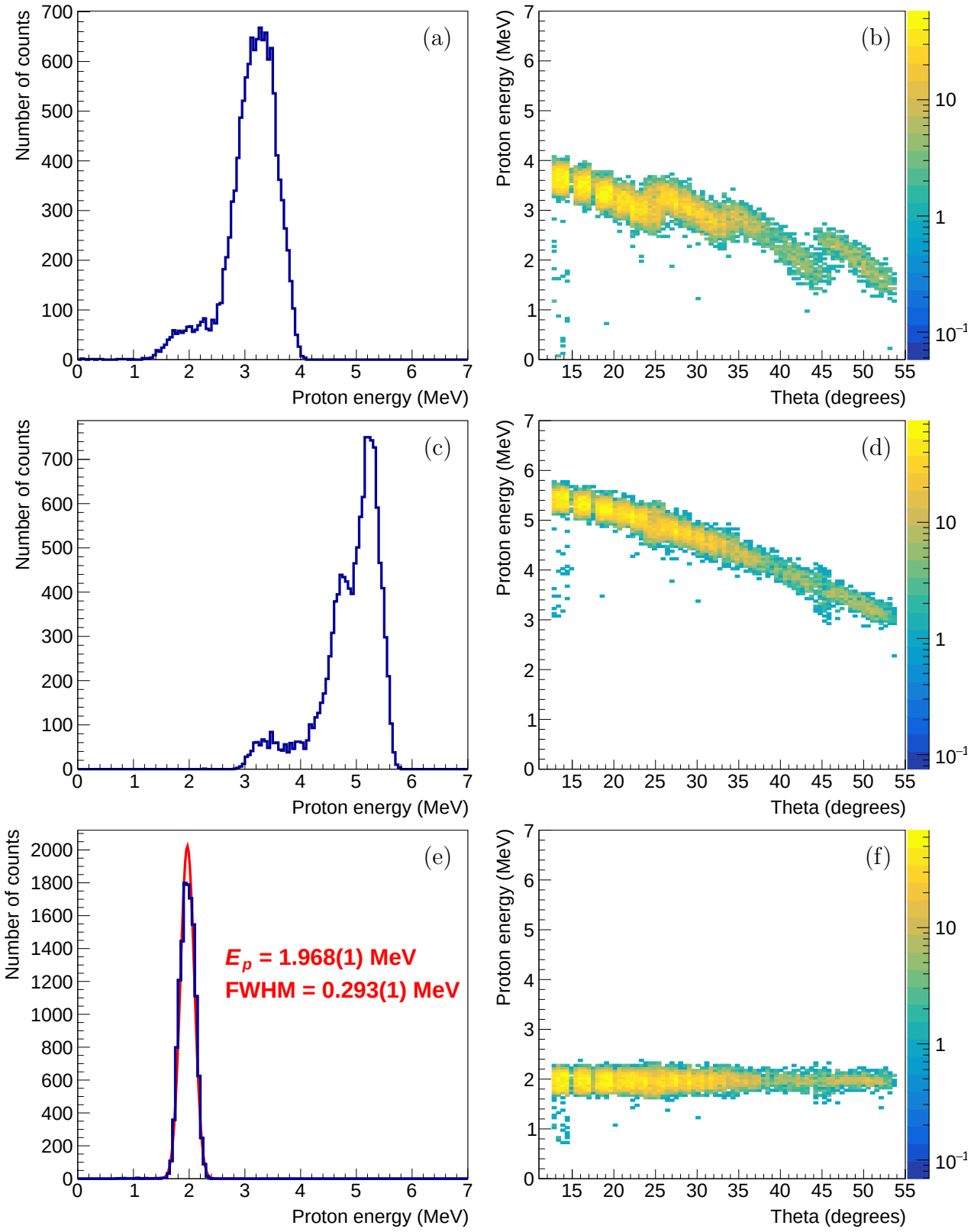

FIG. 5: Results of Geant4 simulations of ^{61}Ga proton emission from a randomized position in the target layer with $Q_{p,\mathrm{in}} = 2.000$ MeV. The model includes all geometric details of the two DSSD and the Ta absorber foils (cf. Fig. 1). Panel (a) shows the energy deposition of the proton in DSSD 1. Panel (b) provides its dependence on the laboratory angle, θ. Panels (c) and (d) show the correction of simulated events for energy loss in the Ta absorber foils done in exactly the same way as was done for experimental data. Panels (e) and (f) provide the proton energy spectrum and distribution after transformation from the laboratory into the center-of-mass frame. Results of a Gaussian least-squares peak fit are included in panel (e).

TABLE II: Coulomb multipole contributions (V_{CM}) to proton-proton two-body matrix elements. The short-hand notations in the first column are "3" for $p_{3/2}$, "5" for $f_{5/2}$, "1" for $p_{1/2}$, and "9" for $g_{9/2}$. All TBME are in keV.

matrix	total angular momentum, J								
element	0	1	2	3	4	5	6	7	8
3 3 3 3	351.0		302.5						
3 3 3 5			5.6						
3 3 3 1			17.1						
3 3 5 5	22.2		3.8						
3 3 5 1			10.5						
3 3 1 1	42.8								
3 3 9 9	-35.0		-12.9						
3 5 3 5		311.9	296.9	279.6	309.2				
3 5 3 1		-0.0	7.9						
3 5 5 5			-2.4		11.0				
3 5 5 1			21.9	6.7					
3 5 9 9			-9.9		-9.6				
3 1 3 1		290.4	314.6						
3 1 5 5			12.3						
3 1 5 1			14.8						
3 1 9 9			-6.7						
3 9 3 9				305.7	270.4	271.4	277.4		
3 9 5 9				-13.0	-3.6	-3.6	2.7		
3 9 1 9					17.8	-18.2			
5 5 5 5	365.1		305.0		282.7				
5 5 5 1			19.0						
5 5 1 1	28.7								
5 5 9 9	-29.9		-4.6		-2.3				
5 1 5 1			306.2	286.3					
5 1 9 9			-9.0						
5 9 5 9			316.6	293.8	273.1	273.3	265.5	308.1	
5 9 1 9					11.4	19.4			
1 1 1 1	320.7								
1 1 9 9	-15.2								
1 9 1 9					277.9	284.0			
9 9 9 9	350.4		302.9		273.3		259.2		261.9

TABLE III: Single-particle energies for JUN45 including electromagnetic spin-orbit ("SO") and radial ("VR") effects and normalized ("n") to keep the SPE centroids at the values of the original JUN45 interaction. See text for details.

Interaction	neutron SPE (MeV)				proton SPE (MeV)			
	$\nu p_{3/2}$	$\nu f_{5/2}$	$\nu p_{1/2}$	$\nu g_{9/2}$	$\pi p_{3/2}$	$\pi f_{5/2}$	$\pi p_{1/2}$	$\pi g_{9/2}$
JUN45 [46]	-9.8280	-8.7087	-7.8388	-6.2617	see left			
JUN45coul_SO	-9.8120	-8.7737	-7.8698	-6.1957	-9.8470	-8.6307	-7.8018	-6.3407
JUN45coul_VR	-9.8280	-8.7087	-7.8388	-6.2617	-10.128	-8.9287	-8.2488	-6.6417
JUN45coul_SOVR	-9.8120	-8.7737	-7.8698	-6.1957	-10.147	-8.8507	-8.2118	-6.7207
JUN45coul_SOVRn	-9.6605	-8.6702	-7.6678	-5.9992	-9.9955	-8.7472	-8.0098	-6.5242